Applied Catalysis B: Environmental 166–167 (2015) 241–250

Contents lists available at ScienceDirect

Applied Catalysis B: Environmental

journal homepage: www.elsevier.com/locate/apcatb

Photodegradation of the anthraquinonic dye Acid Green 25 by TiO_2 immobilized on carbonized avocado kernels: Intermediates and toxicity

Martín M. Dávila-Jiménez [a], María P. Elizalde-González [b,*], Esmeralda García-Díaz [b], Vianey Marín-Cevada [c], Jacquelin Zequineli-Pérez [b]

[a] Facultad de Ciencias Químicas, Universidad Autónoma de Puebla, Ciudad Universitaria, Edif. 105, Puebla, Pue. 72570, Mexico
[b] Centro de Química, Instituto de Ciencias, Universidad Autónoma de Puebla, Ciudad Universitaria, Edif. 103H, Puebla, Pue. 72570, Mexico
[c] Centro de Investigaciones en Ciencias Microbiológicas, Instituto de Ciencias, Universidad Autónoma de Puebla, Ciudad Universitaria, Edif. 103J, Puebla, Pue. 72570, Mexico

ARTICLE INFO

Article history:
Received 15 July 2014
Received in revised form 14 October 2014
Accepted 14 November 2014
Available online 22 November 2014

Keywords:
TiO_2/carbon composite
Acid Green 25
Photocatalysis
Solar irradiation
Product identification
Toxicity

ABSTRACT

The aim of this research was to develop a TiO_2 composite from a waste material in order to study the photocatalytic decomposition of an important residual anthraquinonic dye. Carbon-TiO_2 composites were obtained from carbonized avocado kernels and sols of TiO_2 prepared from NH_4OH and $TiCl_4$ using glycerol as a binder and thermally treating the composites at 500 °C. XRD studies confirmed the anatase phase of TiO_2. SEM images showed isolated TiO_2 agglomerates attached on the carbon surface with a Ti:C ratio of 1:3.3 established by EDS semi-quantitative analysis. The photocatalytic activities of the prepared composites were tested in a decomposition assay of Acid Green 25. Titanium dioxide and the composite eliminated almost 100% of the dye under UV irradiation and the composite demonstrated degradation efficiency under solar light. The reaction was monitored by UV–vis spectrophotometry and by LC-ESI-(Qq)-TOF-MS-DAD, enabling the identification of some intermediate species. No evidence of toxic effects was found in the dye AG25 and its photodegradation products, which were evaluated on the plant growth-promoting bacteria *Azospirillum brasilense*.

1. Introduction

Combinations of TiO_2 and carbon are under active study in the fields of photocatalysis and nanoscience [1]. The most extensively studied combinations include titanium oxide nanoparticles in a carbon matrix and carbon coated with TiO_2. The preparation methods for these materials were reviewed in [1–3]. In recent years, applications of these carbon-TiO_2 materials have gained widespread attention in photocatalysis because (i) the solids are easily recovered after use in a wide range of applications [4] and (ii) synergistic effects occur between TiO_2 and carbon [5]. Whereas carbon doping promotes band-gap narrowing, the presence of carbon in TiO_2 composites promotes the adsorption of pollutants and the creation of catalytic active sites [6], thereby improving photoactivity and selectivity. Furthermore, adding carbon to titania allows for the narrowing of the optical band gap and may extend the light-absorption range of a composite [6]. Adsorption has a particularly significant effect on the susceptibility of dyes to photocatalytic degradation [7].

Carbon-TiO_2 materials are referred to in the literature as doped, hybrid, or composite materials, and most reported preparations have involved several steps. The critical review by Lim *et al.* plainly illustrates several of the practical issues surrounding the preparation of carbon-TiO_2 materials conceived as titanium dioxide supported on activated carbon, *i.e.*, two separate preparation procedures followed by the formation of a composite [3]. The precursors of the composite, *i.e.*, carbon and TiO_2, may be taken directly as finished commercial products [6,8], but carbon can also be impregnated with a titania sol, which gelifies and can be converted to titanium dioxide via thermal treatment, to produce immobilized TiO_2 crystals on carbon particles: a TiO_2/C material. Such immobilization of TiO_2 has been performed, for example, on glass plates by means of a silane binder [9]. Only a few studies have been devoted to the preparation of TiO_2/C materials using lignocellulosic residues such as bamboo leaves [10], pine saw dust [11], maize corncob [12], *Canola* hull [13], and corn straw powder [14] as carbon precursors.

Anthraquinone dyes are considered the second most important class of textile dyes soluble in water. These dyes are characterized

* Corresponding author. Tel.: +52 222 2295500; fax: +52 222 2295525.
E-mail address: maria.elizalde.uap.mx@gmail.com (M.P. Elizalde-González).

http://dx.doi.org/10.1016/j.apcatb.2014.11.034
0926-3373/

by their wide range of colors and durability due to the very stable anthraquinone structure, which is also responsible for their recalcitrant nature. Acid Green 25 (AG25) is a 1,4-diaminoanthraquinone dye with two terminal sulfonic acid groups used to stain wool, synthetic polyamide, and silk. It is consumed in the paper and leather industries but also used as a hair dye ingredient in non-oxidative hair dye formulations at a maximum concentration of 0.3%. The toxicities of AG25 to the single-cell green algae *Selenastrum capricornutum* (50% inhibition) and fathead minnow *Pimephales promelas* ($LC_{50,\,96h}$) are 10 and 6.2 mg L^{-1}, respectively [15]. However, studies of *in vitro* mutagenic effects in bacteria and cultured mammalian cells have not revealed any adverse effect. To mention some acute toxicity of other industrial dyes, six azo dyes showed $LC_{50,\,160h}$ values ranging between 0.13 and 350 mg L^{-1} to *Xenopus* [16].

According to the studies available, AG25 is not irritating to the skin or eyes and did not induce sensitization in one guinea pig experiment. Under the reported conditions, a no-observed-adverse-effect level of 100 mg kg^{-1} bw day^{-1} was deduced for rats after sub-chronic (90 days) oral administration [16]. The 2013 meeting of the Scientific Committee on Consumer Products (SCCP) of the European Union led the SCCP to conclude that the existing information on AG25 is insufficient to assess the safe use of the substance [17].

In work concerning the decolorization and degradation of AG25, the Fenton method [18], the UV/H_2O_2 photooxidative process [19], and photocatalysis in solution with TiO_2 [9,20–23] have been employed. The photocatalytic degradation of AG25 on TiO_2/C materials has not yet been addressed, whereas the adsorption of AG25 from aqueous solutions has been tested using different natural [24–27] and modified adsorbents [28–31]. The activated carbon used in the adsorption of AG25 from aqueous solution has previously been obtained from mango (*Mangífera indica*) seed [25], pineapple (*Ananas comosus*) leaves [31], and Cassava peel [32]. Studies concerning the adsorption of AG25 on composites are limited. Mahmoodi *et al.* reported the preparation of alginate/titania nanoparticles and their use in the adsorption of AG25 solutions at various pH values [33].

Fabbri *et al.* evaluated the degradation of AG25 in aqueous solution using TiO_2 from Degussa as a photocatalyst. The authors identified 19 compounds produced by the detachment of one or two sulfonic groups and/or hydroxylation, followed by the separation of the benzene ring in the molecule of AG25 [23]. Saquib and Muneer identified 1,2-benzenedicarboxylic acid as the main degradation product of AG25 in an aqueous suspension of titanium dioxide [20]. Despite the disclosure of the nature of the photocatalysis products, no toxicity profile during the course of photocatalytic degradation of AG25 has been evaluated in the literature.

Our goal was to develop an inexpensive method for the efficient immobilization of TiO_2 on carbon obtained from avocado kernels. The composite obtained in a single step from a sol prepared from $TiCl_4$ and a glycerol suspension of avocado-derived carbon served to adsorb and decompose the acid anthraquinone dye AG25 both under UV and solar irradiation. This approach provides a better basis for the study of the role of adsorption in the photocatalytic reaction. No mineralization was pursued; instead, we followed the formation of intermediates by LC–MS and evaluated the toxicity of the mixture toward the plant-growth-promoting bacterium *Azospirillum brasilense*.

2. Experimental

2.1. Chemicals

Titanium tetrachloride 99.99% (Alfa Aesar, Ward Hill, MA, USA) and glycerol GR (87%, Merck, Darmstadt, Germany) were used as reagents. Ammonium hydroxide (28%, Aldrich, St. Louis, MO, USA) was used for sol formation. Avocado kernels [34,35] were used as a carbon source. They exhibited a specific surface area of 53 m^2 g^{-1}, a 58% of porosity, an apparent density of 0.39 g cm^{-3}, a moisture and ash content of 6.8% and 2.2%, respectively. The organic and inorganic composition (%) of the avocado kernels was as follows: C (44.6), H (6.3), N (0.7), O (48.4), Na_2O (2.1), MgO (7.9), Al_2O_3 (2.4), SiO_2 (38.4), K_2O (44.8), CaO (3.1). The commercial dye AG25, CI 61570, was provided by Clariant Mexico SA de CV (Naucalpan, Edo. de Mexico, Mexico). The purity of the dye determined by elemental analysis was 83.5%. Degussa P-25 TiO_2 was used in the toxicity experiments. 2-Amino-5-methylbenzene sulfonic acid and $Ba(OH)_2$ from Aldrich (St. Louis, CA, USA) were used as a chromatographic standard and as a precipitating agent, respectively.

2.2. Immobilization of TiO_2 on carbon

The carbon precursors were prepared from avocado kernels (0.5 mm sieved particles) dried at room temperature for 24 h and at 50 °C for 48 h. Then, the particles were pre-activated according to a previously reported procedure [35]. Three carbon samples (C1, C2 and C3) were obtained in a horizontal tubular furnace Carbolite (Parsons Lane, Hope, United Kingdom) with a quartz reactor.

Three TiO_2/C composites (CATI-1, CATI-2, and CATI-3) were fabricated as follows. Fresh sols of TiO_2 were prepared previously for each composite by adding NH_4OH to $TiCl_4$ dropwise under stirring. The blank TiO_2 material prepared by this methodology exhibited a specific surface of 59 m^2 g^{-1} and a band gap of 2.6 eV and consisted of 87% anatase and 13% rutile after calcination at 500 °C. The carbon samples (200 mg) C1, C2, and C3 with a sieved particle size 0.42 mm were stirred separately in 2 mL of glycerol for 24 h. Then, a sol (2 mL) of TiO_2 was added dropwise. The resultant homogeneous suspension was maintained at 20 °C for 48 h in a combustion boat. Then, the TiO_2/C composites were calcined in air using the following heating rates: (1) from room temperature to 300 °C at 4 °C min^{-1} and (2) from 300 to 500 °C at 2 °C min^{-1}. The composites were isothermally held at 300 and 500 °C for 1 h. The oven was then allowed to cool to room temperature.

2.3. Characterization of the composites

XRD measurements were carried out using a STADI P automated transmission diffractometer from STOE (Darmstadt, Germany) with Cu Kα_1 radiation (α = 1.5406 Å) and a 6° linear position sensitive detector (PSD). The alignment was verified using a silicon standard. Data were collected over the 2θ range of 5–60°, with a step size of 0.5° and a measurement time of 50 s per step. The diffractogram was smoothed by the Savitsky-Golay method. Diffuse reflectance spectra of the samples (1:30 in $BaSO_4$) were recorded at room temperature using an Ultra-Low Straylight Fiber Optic Spectrometer from Avantes (Connecticut, USA) coupled to a reflection probe at 45°. The morphology and surface composition of the samples were determined using an Oxford Instruments INCAX-act Energy 350 EDS spectrometer coupled to a JEOL JSM 6610 LV scanning electron microscope (SEM). Four samples were analyzed, and the elemental composition was averaged. The BET surface area was measured by nitrogen adsorption at 77 K using an Autosorb-1 from Quantachrome (Florida, USA) after out-gassing at 573 K for 12 h. The specific surface was calculated using the Brunauer–Emmett–Teller (BET) equation, and the pore size distribution was estimated by the Barrett–Joyner–Halenda method (BJH). The extent of microporosity was calculated using the micropore volume obtained from the adsorption isotherms of nitrogen and the application of the Dubinin–Radushkevich equation. The density of the dry materials was determined in triplicate using a gravimetric method with tapered test tubes. The point of zero charge pH_{pzc} was determined

by potentiometric mass titrations under a N_2 atmosphere and at a constant temperature (23 °C ± 0.1). Potentiometric titrations were performed using a Tritando Metrohm 809 (Riverview, FL, USA) to determine the final pH values.

2.4. Adsorption experiments

Adsorption tests were performed at 25 °C in thermostated batch experiments. The solid materials, carbon, and TiO_2/C composites with a particle size of 0.125 mm were dried for 24 h at 100 °C. Then, 50 mg of each material was weighed into polycarbonate cylindrical cells with a lid and contacted with 1.5 mL of AG25 solutions with concentrations in the range of 25–300 mg L^{-1}. For the measurement of the adsorption isotherm of AG25 solutions on Degussa TiO_2, the concentrations varied in the range of 50–1000 mg L^{-1}. The pH was not adjusted and was measured to be 5.8 in deionized water. The solution that resulted from the adsorption equilibrium obtained after 24 h was separated from the exhausted adsorbent and centrifuged (12,000 rpm) and then analyzed with a UV–vis Beckman DU 7500 spectrophotometer at 642 nm.

2.5. Photocatalytic experiments

For the irradiation experiments performed on the composites and TiO_2 (Degussa P25), two set-ups were used: A 15-mL temperature-controlled quartz reactor from Ace Glass Inc. (Vineland, NJ, USA) was used for experiments involving irradiation at 254 nm, and a beaker was used for experiments involving solar irradiation. The commercial TiO_2 from Degussa was used for comparison because it exhibited similar properties as the TiO_2 we prepared using $TiCl_4$. Both Degussa and our TiO_2 were a mixture of anatase (>80%) and rutile. The band gap of Degussa's and our titanium dioxide was 3.1 and 2.7 eV, respectively. Degussa TiO_2 exhibited 60 m^2 g^{-1} and ours 59 m^2 g^{-1}.

A 2 1/8-in. Pen-Ray light source (5.5 W) from Ultra-Violet Products (Upland, CA, USA) was immersed into the reactor in a quartz jacket. The reactor was equipped with a water jacket to avoid IR irradiation of the lamp and to control the temperature (25 °C) of the solution. The entire assembly was enclosed in a dark chamber, and the lamp was switched on after 30 min to establish the adsorption equilibrium. In each experiment, 10 mg of the composite was added to 5 mL of a solution containing 50 mg L^{-1} of AG25. Aliquots were collected at regular time intervals during irradiation and were centrifuged for 45 min before analysis.

Solar photocatalytic experiments were performed on 26th November 2013 in the garden of the Institute of Sciences at the Universidad Autónoma de Puebla, Puebla, Mexico (19°02′43"N 98°11′51"W), in 50-mL closed glass beakers fitted with a needle valve. The reported irradiance value was 17 MJ m^{-2}. Each series consisted of a blank, a control sample kept in the dark, and the exposed samples (500 mg of composite in 15 mL AG25 solutions with a concentration of 50 mg L^{-1}).

Aliquots of all AG25 solutions subjected to photocatalytic testing with composites and TiO_2 (Degussa) were analyzed using a Hach DR 5000 UV–vis spectrophotometer over the wavelength range of 200–800 nm. In a target experiment lasting 75 min, the evolution of CO_2 was monitored by the precipitation of $BaCO_3$ by bubbling the stream coming from the beaker into a $Ba(OH)_2$ solution contained in a tapered test tube.

2.6. Evaluation of toxicity in bacteria

Toxicity was screened for AG25 aqueous solutions with concentrations of 30 and 100 mg L^{-1} and for AG25 (30 mg L^{-1}) solution subjected to irradiation in presence of TiO_2. Also a solution without dye (control) and a solution supplemented with NaCl (250 mM) were tested as positive and negative controls, respectively. The initial AG25 solutions were sonicated for 20 min to ensure homogeneity, and the pH was not adjusted. The irradiation experiments were performed at 254 nm at 50 °C with 30 mg L^{-1} AG25 (150 mL) and TiO_2 (Degussa) in a 200-mL reactor using a magnetic stirrer. The glass body of the vertical tubular reactor had an internal diameter of 4.5 cm and a height of 15 cm. The pen lamp was immersed in the reactor in a quartz jacket. The reactor was maintained in the dark for 30 min to establish the adsorption equilibrium before the lamp was switched on. The same lamp described in Section 2.5 was used.

The plant-growth-promoting bacterium *A. brasilense* DSM 1843 was used to assess the toxic properties of the final solution collected from the photodegradation experiment described above. Bacteria were cultured by inoculating 100 μL of bacteria in cultures and controls separately in 30 mL of Luria Broth (LB) and incubating them at 150 rpm for 24 h at 30 °C. An aliquot (1 mL) was sampled from each culture at 2, 4, 6, 10, and 24 h after inoculation. The bacterial cultures were serially diluted with 10 mM $MgSO_4 \cdot 7H_2O$. Serial dilutions were plated on Congo agar in three replicates and incubated for 24 h.

For the acetylene-reduction assay, *A. brasilense* DSM 1843 was grown in 30 mL of modified LB (without yeast extract) under rotary agitation (120 rpm) for 18 h at 30 °C in 125-mL Erlenmeyer flasks. The culture was washed three times with sterile 10 mM $MgSO_4 \cdot 7H_2O$ and centrifuged at 13,000 rpm for 10 min. The optical density of the bacterial culture was adjusted to 0.05 at 620 nm, corresponding to 1.0×10^6 CFU/mL^{-1}. The same trials used in the bacterial survival assay were assessed in nitrogen-free semisolid malate medium (NFB): 25 μL of the inoculum and incubation without movement at 30 °C for 48 h. Nitrogenase activity was evaluated by the acetylene reduction assay (ARA) as reported by Hara et al. [36]. Following 24 h of incubation, the cotton plugs were replaced by suba seal septa, the gas phase in the headspace was replaced by injecting pure acetylene to a final concentration of 10% (v/v). Ethylene formation was measured using a gas chromatograph Varian model 3300. All of the assays were performed with three replicates. Nitrogenase activity was expressed in nanomoles ethylene per hour per milliliter of semisolid medium. A quantitative determination of bacterial population was also performed for assessing the effect of AG25 dye on *A. brasilense*. A one way ANOVA analysis of the population was performed in the different growth media with the null hypothesis that the means of all the populations are equal. With an interval of confidence of 95%, the Tukey and Fisher tests were performed. All statistical analyses were performed using the data analysis and graphing software OriginPro 8.5.

2.7. Analysis of photocatalysis products

For the identification of photodegradation products, aliquots were collected at different time intervals and analyzed by LC-ESI-(Qq)-TOF-MS using an LC–MS instrument (Series 1260 chromatograph coupled with an ESI-(Qq)-TOF-MS 6520 detector from Agilent Technologies, Santa Clara, CA, USA). The separation was carried out at 25 °C using a Nucleodur EC C18 Isis (5 μm, 250 × 4.6 mm) column from Macherey–Nagel (Düren, Germany). Gradient elution at 1 cm^3 min^{-1} with a methanol–water (10–90%) mobile phase between 0 and 20 min and 90% methanol up to 25 min was performed. Both solvents contained 40 mM acetic acid-triethylamine reagent from Fluka (Buchs, Switzerland) as an ion pair agent. To methanol (Burdick-Jackson, Muskegon, MI, USA), 0.1% HCOOH from Aldrich (St. Louis, CA, USA) was added. The injection volume was 50 μL.

ESI-TOF-MS was performed in the negative ionization mode (ESI(−)) with nitrogen as the drying gas at 11 dm^3 min^{-1}, applying a TOF fragmentor voltage of 175 V, a capillary voltage of 3500 V

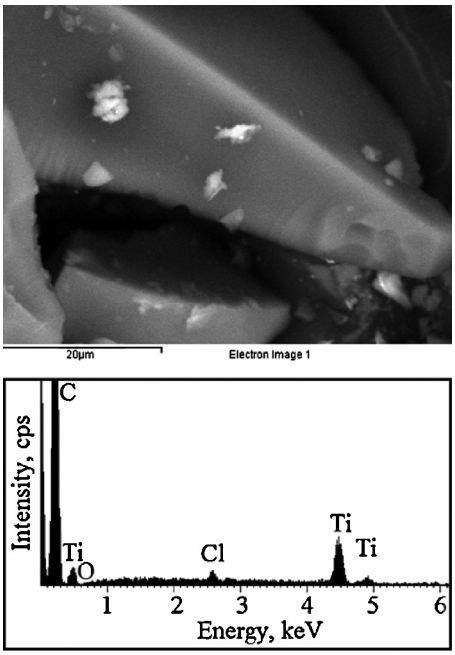

Fig. 1. Scanning electron micrograph of the composite CATI-3 and respective EDS spectrum.

over an *m/z* range of 50–700, a gas temperature of 350 °C, and a nebulizer pressure of 60 psi. For the MS/MS analysis, ESI-Qq-TOF-MS was used in the negative ionization mode, applying a CE of 30 V over an *m/z* range of 50–300 and an isolation width of 1.3 *m/z*. Total energy calculations were performed with the software ChemSite Pro Version 8.1 from ChemSW (Fairfield, CA, USA).

3. Results and discussion

3.1. Characterization of the TiO_2/C composites

The TiO_2/C composites were black powders. Their density was higher than that of the corresponding carbons (see Table 1). Carbons with different pH_{pzc} values were obtained due to the preparation method. However, all three composites presented similar neutral values of pH_{pzc} ~7.

Fig. 1 shows an SEM image of the CATI-3 sample. The morphologies of the prepared composites were similar and consisted of irregular particles recovered by a smooth carbonaceous film. Isolated TiO_2 agglomerates (<10 µm) were attached to the surface of the particles. By using glycerol, Sreethawong *et al.* observed uniform TiO_2 nanoparticles in the form of clusters [37]. The lower part of Fig. 1 shows the surface composition results obtained from the EDS spectra of CATI-3 and indicate the presence of mainly titanium and carbon. Oxygen was observed in low concentrations as part of the TiO_2, whereas Cl was a residue of the $TiCl_4$ used as precursor in the preparation of the sol of TiO_2. The semi-quantitative EDS analysis revealed that the Ti:C ratio in the composite materials was, on average, 1:3.3. In studies of the adsorption and degradation of AG25, immobilized TiO_2 particles were observed to entirely cover the surface of sodium alginate [33] and glass plates [9]. Our SEM images suggest that adsorption and photocatalysis phenomena occurred simultaneously due to the low loading of TiO_2 on carbon.

The composites prepared by immobilization of TiO_2 exhibited crystallinity (see Fig. 2) after calcination at 500 °C. The peaks were broad due to the presence of carbon, and of low intensity, but produced anatase-type TiO_2. This result suggests that glycerol promoted crystallization at a relatively low calcination temperature, as previously described by our group [38]. The main diffraction peak of the anatase phase (1 0 1) was convoluted with the carbon peak of the plane (0 0 2) at a 2θ value of 25.3° (see Fig. 2). The basal plane of carbon (10) also appeared at a 2θ value of 45.3°.

The UV–vis diffuse reflectance spectra of the composites are shown in Fig. 2B. The carbon samples C1 and C2 and the respective composites showed enhanced absorbance in the visible range relative to TiO_2, fact which is intrinsic in carbon materials. Carbons absorbed more than their respective composites as clearly observed in the case of C2 and CATI-2. The absorption of the composites CATI-2 and CATI-3 in the range $\lambda > 400$ nm was similar and higher than that of the composite CATI-1.

The immobilization of TiO_2 on carbon in the presence of glycerol affected the textural characteristics of the respective carbon samples prepared by using avocado kernels, as demonstrated by measuring the N_2 adsorption–desorption isotherms. The specific surface area (S_{BET}) and other textural parameters are listed in Table 1. According to the IUPAC classification system, the three carbon samples C1, C2, and C3 (Fig. 3A) displayed a hybrid isotherm of types I and II, which are typical for materials with a considerable degree of microporosity. These nitrogen adsorption isotherms contrasted significantly with the type III isotherms exhibited by the composites. As expected, the presence of crystalline TiO_2 drastically decreased the specific surface areas (see S_{BET} in Table 1) of the composites due mainly to the obstruction of the carbon micropores by the film formed by the carbonized glycerol. This circumstance differs greatly from that of the carbon/TiO_2 composites prepared by Velasco, in which S_{BET} was not observed to be correlated with the relative amounts of carbon [39]. Regardless of the effect of glycerol on the specific surface magnitudes, we aimed to firmly immobilize low amounts of TiO_2 on carbon. The pore size distribution in the composites revealed a broad distribution of mesopores (Fig. 3B, left axis), whereas in the carbons, most nitrogen was adsorbed in the micropores. These results suggest that the carbonaceous film was non-porous (see Fig. 1) and that the TiO_2 crystallites and their clusters gave rise to large mesopores. The composite CATI-1 exhibited a significant low S_{BET} (Table 1) corresponding to a non-porous–macroporous solid. Accordingly, its pore size distribution is broad. The other composites, CATI-2 and CATI-3 presented similar adsorbed volumes and S_{BET} and consequently, their average pore diameter is comparable (Table 1).

3.2. Adsorption of AG25 solutions

The dye AG25 is also sold under the names Acid Green Anthraquinone, Alizarin Cyanine Green F, Japan Green 201, and D&C Green No. 5. The commercial dye AG25 used in this work consisted of a mixture of isomers, as indicate by their LC–MS spectra, which will be discussed in the next section. Thus, the adsorption, photodegradation, and toxicity studies of the dye concern a bi-component mixture subjected to the corresponding processes. Fig. 4 illustrates the isotherms describing the adsorption of the commercial product of AG25 onto TiO_2, the avocado carbon sample C3 and on the composite CATI-3 without any adjustment. The corresponding Langmuir constant k_L and saturation capacity q_m values were calculated by the linear form of the Langmuir equation, and the respective results were 296 L g^{-1} and 11.4 mg g^{-1} on TiO_2, 33.3 L g^{-1} and 1.03 mg g^{-1} on carbon and 52.7 L g^{-1} and 0.41 mg g^{-1} on the composite CATI-3. The k_L value is comparable to that reported for a walnut adsorbent [24]. Compared with the values reported in the literature [28–30], our materials were saturated with low amounts of AG25. The semiconductor TiO_2 adsorbed a tenfold amount of AG25 in comparison to the composite CATI-3 and the carbon C3, as seen from the scale in Fig. 4. The composite adsorbed approximately the half of the amount of AG25 adsorbed per unit of mass by the carbon. Due to the differences in the magnitude of the specific surface area, the composite retained almost ten

Table 1
Physical and textural properties of the avocado seed carbons and the TiO_2/C composites.

Sample	ρ (g cm^{-3})	pH_{pzc}	S_{BET} (m^2 g^{-1})	Micropore volume (%)	Average pore diameter (nm)
C1	0.16	9	890	54	2.8
C2	0.14	6	1630	38	3.6
C3	0.31	10	1240	59	2.7
CATI-1	0.52	7.1	1	–	90
CATI-2	0.26	7.0	40	–	5.9
CATI-3	0.25	7.2	35	–	8.7

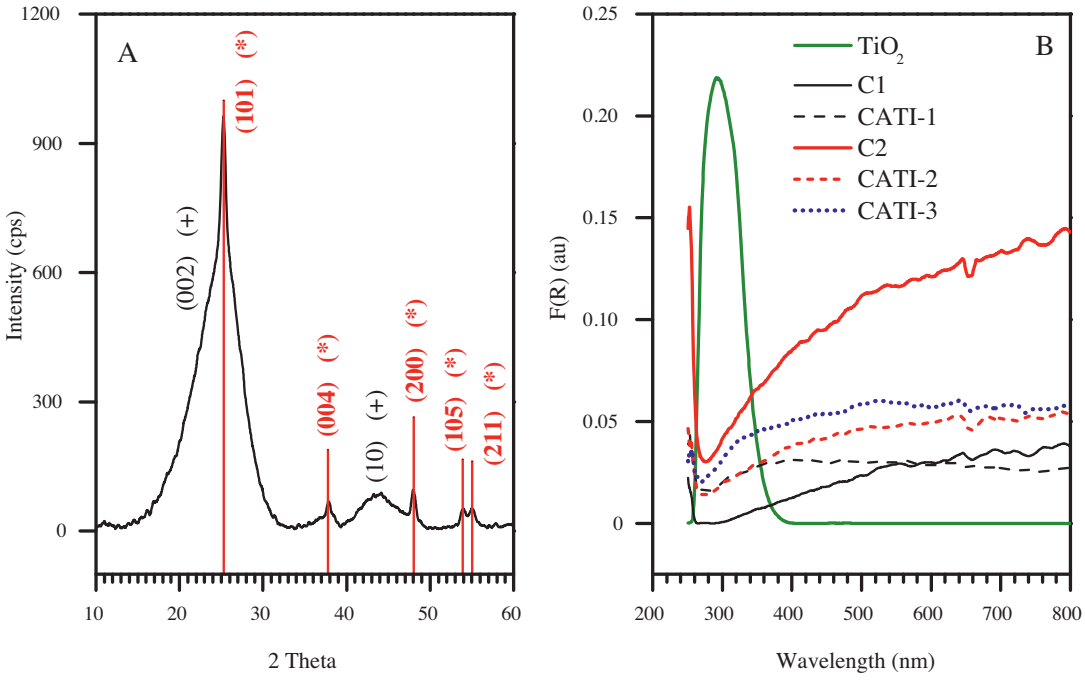

Fig. 2. X-ray powder diffraction pattern of the composite CATI-3 showing the peaks of the planes (lines) of the anatase phase (*) and of the planes (0 0 2) and (10) of carbon (+) (A). UV–vis diffuse reflectance spectra of bare TiO_2, carbon, and composite samples (B).

times the mass of AG25 per square meter relative to the carbon, as shown in the lower graph of Fig. 4.

Finally, we aimed to demonstrate the relative adsorption affinities of the semiconductor TiO_2, and their composites upon the adsorption of AG25. In agreement with the adsorption isotherms in Fig. 4, when a 50 mg L^{-1} solution of commercial AG25 was measured after 60 min of contact with the three different materials, the band at 600–650 nm in Fig. 5A indicated that adsorption occurred on the Degussa TiO_2 to a greater extent than on the composite CATI-3 under the same conditions. This explains the isotherm depicted in the lower graph of Fig. 4, *i.e.*, adsorption of AG25 per square meter is greater on the composite than on carbon despite the low amount of TiO_2. In general, the presence of TiO_2 improved the adsorption capacity of the composites relative to carbon.

3.3. Photodegradation of AG25 under UV irradiation

Fig. 5B depicts the UV–vis spectra of the irradiated AG25 solutions at 254 nm after 30 min of contact with the composite CATI-3 and Degussa TiO_2. Successfully, the prepared TiO_2/C composite exhibited the same degradation efficiency toward the dye as TiO_2, regardless of the low load of the semiconductor in the composite. For the identification of intermediates, we monitored a 50 mg L^{-1}

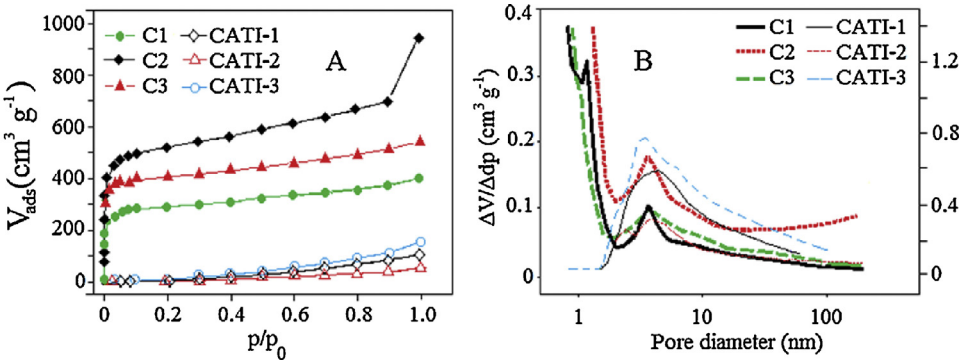

Fig. 3. Nitrogen adsorption isotherms (A) at 77 K for the carbon samples C1, C2, and C3 and the CATI composites. Pore size distribution curves (B) of the studied samples.

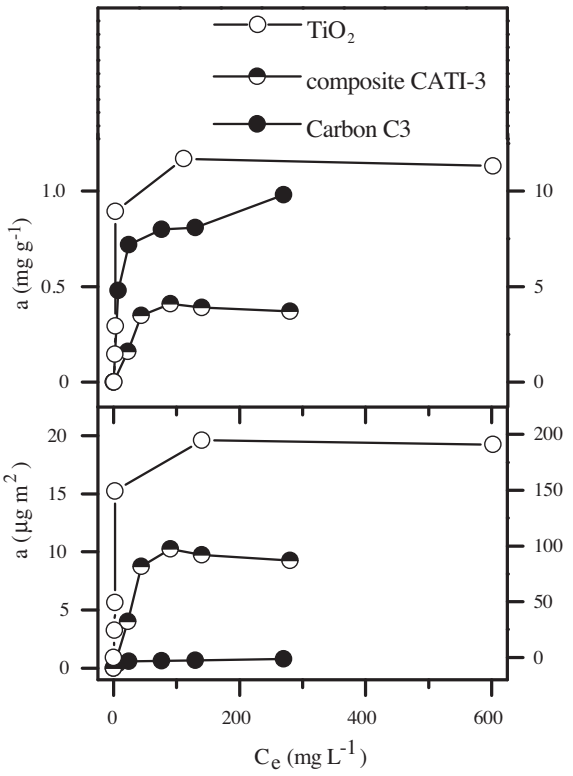

Fig. 4. Adsorption isotherms of AG25 from aqueous solution on carbon sample C3, composite CATI-3 and Degussa TiO_2 at 25 °C. Equilibrium time 24 h, solid dosage of 30 g L^{-1}. Upper graph shows the adsorbed amount in mg g^{-1} and the lower graph in μg m^{-2}. Carbon C3 and composite CATI-3—left axis, Degussa TiO_2 right axis.

AG25 solution stirred with TiO_2 and irradiated at 50 °C with a UV lamp. Fig. 6 shows the results of the experiment.

The LC–MS chromatogram of the stock solution of AG25 (Fig. 6A) indicated that the commercial product consisted of a mixture of two isomers in a ratio 1:1.7, whose ESI-MS spectra exhibited molecular ion masses $[M-H]^-$ of m/z 577.0738 ($\Delta m/z$ −1.21) and 577.0744 ($\Delta m/z$ −0.17) for the isomers *a* and *b*, respectively. It is likely that the sulfonation of the p-toluidine moiety in the synthesis precursor of AG25, the dye solvent green 3, results in the formation of isomers because the benzene rings are more reactive than the anthraquinone system, but sulfonation does not occur preferentially on either of the positions 1,1′ or 6,6′ (or 3,3′ and 4,4′) of each of the two p-toluidine moieties. As remarked by Hisaindee *et al.* [40], the LC–MS technique is, however, unable to distinguish between isomers unless standards are available. Our total energy calculations indicated that the 1,6′- and the 6,6′-bis(5-methylsulfonate)

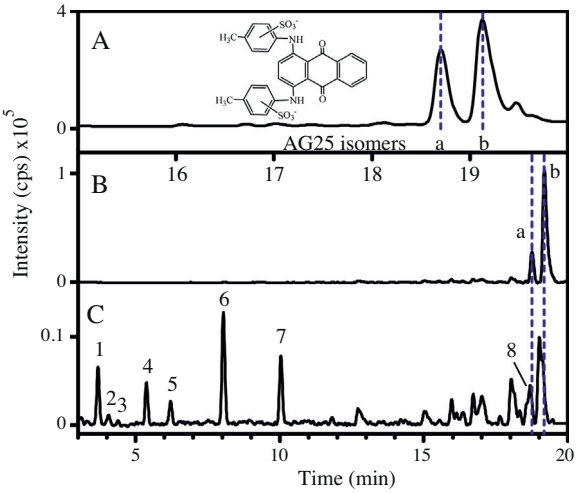

Fig. 6. TIC obtained from the LC–MS analysis of (A) the stock solution of the dye AG25 (30 mg L^{-1}) and after (B) adsorption in the dark and (C) photocatalytic reaction (90 min) with the composite CATI-3. Chromatographic conditions described in the experimental part. Peaks correspond to the identified products P1–P10 gathered in Table 2.

isomers are more stable than the 1,1′-isomer and might correspond to the a and b isomers. The two small peaks eluting after the AG25 pair of peaks most likely correspond to less polar synthesis byproducts or to the third isomer. We could not assess a feasible mass spectrum for these peaks because the peak tailing affected the resolution.

After the adsorption of AG25 on TiO_2, the relative area of the peaks that appeared within 18.5 and 19.5 min indicated first that both of the isomers were adsorbed on TiO_2 in the dark and that isomer *a* was adsorbed to a greater extent than isomer *b* because their ratio became 1:4.4 (Fig. 6B).

At least six new peaks of considerable intensity eluted prior to the appearance of the dye peak in the aliquot chromatogram (Fig. 6C) analyzed during the photocatalytic experiment. The peaks numbered in Fig. 6C correspond to the intermediate products obtained using TiO_2 and exhibit a defined isotopic pattern. Table 2 presents the retention times, exact masses of the molecular ions (m/z), error values ($\Delta m/z$), and proposed structure for eight of the products detected in Fig. 6C. The mass error accuracy of the proposed structures was less than 5 ppm. Furthermore, the identity of 2-amino-5-methylbenzene sulfonic acid (peak **6**) was confirmed by retention-time matching and the MS spectrum of a reagent-grade compound. The accurate identification of the aforementioned structures indicates that under the applied photocatalytic conditions (6 h of irradiation at 254 nm), TiO_2 did not tend to completely decompose the dye molecule. The products listed

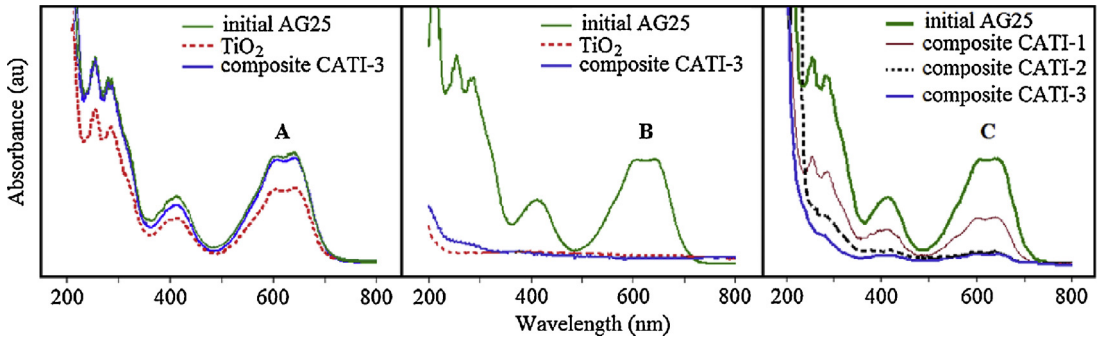

Fig. 5. UV–vis spectra of AG25 aqueous solutions after adsorption (A) and photocatalytic experiments with UV (B) and solar (C) irradiation in presence of Degussa TiO_2 (A and B) and composites (A–C) after 60 (A) and 30 min (B and C) of contact. Initial concentration of AG25: 50 mg L^{-1}, dosage: 2 g L^{-1}.

Table 2
Retention time and possible structures identified by LC-ESI-Qq-TOF-MS as products of AG25 after 90 min of photoreaction at 254 nm.

Peak	t_R (min)	Formula	IUPAC name	$[M-H]_{exper}$	$[M-H]_{calc}$	Δm [ppm]
1	3.69	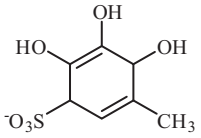	2,3,4-Trihydroxy-5-methylcyclohexa-2,5-diene-1-sulfonate	221.0134	221.0125	4.1
2	4.05	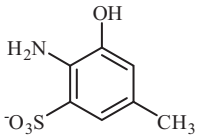	2-Amino-3-hydroxy-5-methylbenzenesulfonic acid	202.0170	202.0179	−4.5
3	4.37	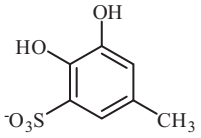	2,3-Dihydroxy-5-methylbenzenesulfonate	203.0025	203.0020	2.5
4	5.36	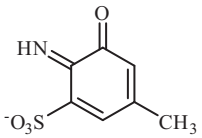	6-Imino-3-methyl-5-oxocyclohexa-1,3-diene-1-sulfonate	200.0028	200.0023	2.5
5	6.21	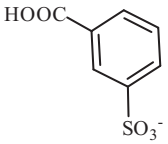	3-Sulfobenzoic acid	200.9905	200.9863	−3.5
6	8.05	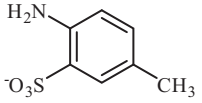	2-Amino-5-methylbenzenesulfonate	186.0227	186.0230	−1.6
7	10.14	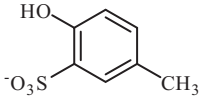	2-Hydroxy-5-methylbenzenesulfonate	187.0076	187.0071	2.7
8	18.69	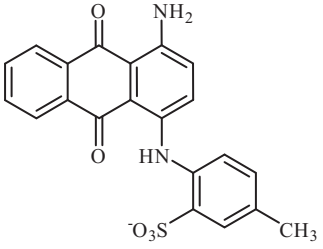	2-((4-Amino-9,10-dioxo-9,10-dihydroanthracen-1-yl)amino)-5-methylbenzenesulfonate	407.0715	407.0707	2.0
AG25	18.76 (isomer a) and 19.12 (isomer b)	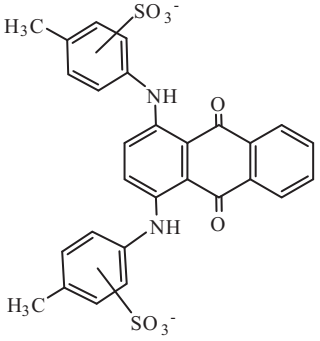	disodium 2,2′-(9,10-Dioxoanthracene-1,4-diyldiimino)bis(5-methylsulfonate)	577.0745	577.0738 (isomer a) and 577.0744 (isomer b)	−1.21 (isomer a) and −0.17 (isomer b)

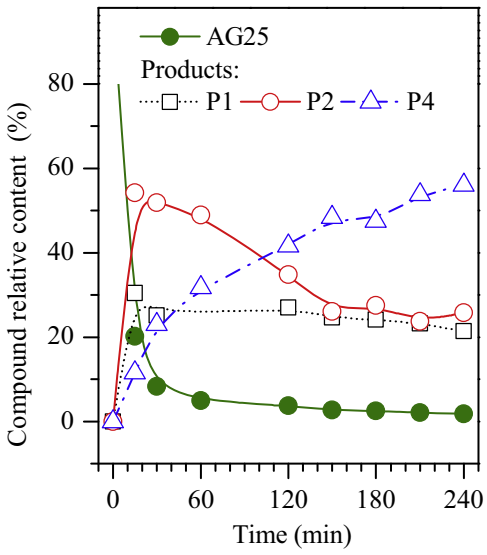

Fig. 7. Kinetic curves of AG25 (30 mg L^{-1}) and three decomposition products produced during photocatalytic decomposition on TiO_2 at 254 nm and 50 °C.

in Table 2 indicate that breakage of the AG25 molecule yields the 5-methyl-benzenesulfonic acid moiety with different degrees of hydroxylation. Moreover, intermediate 7 carries a hydroxyl group derived from intermediate 6 by oxidation. Previous studies of the photocatalytic degradation of AG25 in the presence of anatase [9,20,23] have reported the formation of different products than those observed in our study: benzene-1,2-dicarboxylic acid [20], benzene-1,3-dicarboxylic acid and hydroxylated anthraquinone systems [23], and phenol**,** 4-formylbenzoic acid and hydroxyphthalic acid [9]. By contrast, the sulfonated intermediates with $m/z < 221$ detected in our study have not been reported for the degradation of AG25. Other researchers have reported to have nearly achieved mineralization of the dye after 4 and 12 h using commercial anatase (not Degussa) at 360 [23] and 254 nm [9]. However, the Degussa TiO_2 was observed to be the most efficient photocatalyst toward AG25 when different titanium dioxide products were compared [20]. Only one compound reported by the authors cited above [9,41], with a mass m/z of 407, agreed with the m/z value (peak **8**) observed by us. This compound was produced by the leakage of one benzenesulfonic ring in the AG25 molecule and might be responsible, together with the residual AG25 dye, for absorption in the visible-light range. This observation suggests that mistakes may occur when the degradation and reaction kinetics are measured using the spectrophotometric method. Only LC allows for the determination of the real concentration of the dye at a given reaction time [38]. Furthermore, we observed that isomer *b* was degraded to a greater extent than isomer *a* because the respective peak was nearly extinguished. In the retention time region where the AG25 peaks appeared (Fig. 6C) we observed peak 8 and a peak very close to isomer b. However, the mass spectra of both peaks differed from those of the AG25 isomers. Unfortunately, no structure could be assigned to the peak before the peak of isomer b and of some other small peaks in the retention time range within 12.5 and 18.5 min.

The progress of the decomposition reaction is shown in Fig. 7. Most of the compounds were observed to be present in all samples. As the reactions proceeded, compound P4 (peak 4 in Table 2) was produced to a greater extent, and the curves corresponding to the prepared composites were similar and exhibited the behavior of consecutive reactions.

3.4. Photodegradation of AG25 under solar irradiation

In the photocatalytic degradation of dyes in wastewater, the azo group has been studied extensively. The most widely used semiconductor catalysts are TiO_2 and doped TiO_2, applied under UV irradiation [41]. Xu *et al.* [42] demonstrated that for the azo dye Reactive brilliant X-3B, the apparent degradation rate constant was enhanced under visible illumination using lanthanide-doped TiO_2 due to a higher adsorption capacity. Because we demonstrated the adsorption and affinity characteristics between AG25 and the composite, the photocatalytic degradation of the dye under solar irradiation was explored. Fig. 5C shows the spectra demonstrating the decolorization of the AG solution in contact with different composites. The degree of removal obtained with different composites likely varied due to the magnitudes of the S_{BET} (see Table 1) and the amount of immobilized TiO_2 exposed to irradiation. The extent of decolorization was 63% using the composite CATI-1 and approximately 92% using the composites CATI-2 and CATI-3. The composites CATI-2 and CATI-3 with similar S_{BET} exhibited almost the same efficiency under solar light (Fig. 5C). Their performance was slightly lower than that of TiO_2 under UV irradiation (judging from the bands at 400 and 600 nm). This can be understood taking into account that only ca. 5% of the UV high-energetic irradiation is contained in the solar light. Furthermore, part of the radiation emitted by the light source is absorbed by the molecule to decompose, leaving less light to the material for which the energy is also used to create charge carriers.

The formation of CO_2 during these experiments indicated a high degree of mineralization. However, the remaining bands in the UV-range ($200 < \lambda < 300$ nm) indicated the formation of residual decomposition products coexisting with low concentrations of AG25 after 30 min of irradiation.

For anthraquinonic dyes, the persistence of aromatic compounds has also been reported after ozonation [43]. As described in Section 3.3, the compounds formed in the presence of TiO_2 consist of aromatic rings, which might absorb light in the UV range. In addition, compound eluted as peak **8** corresponds to the loss of one benzenesulfonic moiety. This compound, together with the residual AG25, might be responsible for the lasting color.

3.5. Toxicity profiling

A few studies have investigated the toxicity profiles of dyes during the course of photocatalytic degradation [44]. We propose a different biological model for evaluating toxicity. The toxicity test was conducted using *A. brasilense*, a free-living nitrogen-fixing bacterium. Because of the action of the nitrogenase complex, *Azospirilla* have the ability to convert atmospheric nitrogen into ammonium under microaerobic conditions at low nitrogen levels. The nitrogenase enzyme also reduces acetylene to ethylene and both gases can be quantified using gas chromatography [45].

There was no critical variation in the nitrogenase activity when *A. brasilense* cultures were exposed to the AG25 dye and its photoproducts. The evidence is provided by the conversion yields: 38 nmol h^{-1} mL for the control, 44 nmol h^{-1} mL for the dye, and 38 nmol h^{-1} mL for the photoproducts in solution. It was established that the most active strains of *A. brasilense* have an ability to reduce C_2H_2 of 25–50 nmol h^{-1} mL and those with low activity, fewer than 20 nmol h^{-1} mL [46]. On the basis of this microbial toxicity study (24 h), the presence or absence of the AG25 dye (100 mg L^{-1}) did not show any effect on the N_2-fixation of *A. brasilense* cultures.

In presence of AG25 (30, 100 mg L^{-1}, and mixture of photoproducts), Azospirillum showed a significant enhancement of growth after the early phase of 8 h. Several species like *Rhizobium* sp., *Bradyrhizobium* sp., *Pseudomonas* sp., *Azospirillum* sp., *Ralstonia*

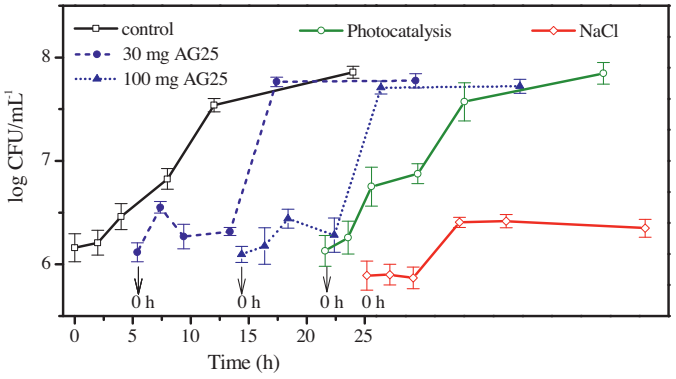

Fig. 8. Evaluation of the specific growth rate of *Azospirillum brasilense* DSM 1843 in NFB medium and incubated at 30 °C at 150 rpm in different trials. Time axis shifted in each curve for clarity.

sp., *Burkholderia* sp. or *Flavimonas* oryzae present chemoattraction towards aromatic compounds, explosives, aliphatic hydrocarbons and herbicides. Experimental evidences have been gathered to suggest that the physiological relevance of chemoattraction to pollutants is decisive, demonstrating that these compounds serve as carbon and energy sources [47].

Additionally, a diauxic growth curve was observed when Azospirilla were in contact with the photoproducts. Depletion of the sources that are metabolized readily occurs first. Then, the organic compounds such as anthraquinone and sulfonated derivatives are metabolized for their incorporation into biosynthetic processes. Fig. 8 presents these results and shows that AG25 is not toxic under these evaluation conditions. The Tukey and Fisher tests performed on the population growth showed that the NaCl treatment mean was significantly different. This means that the salts can affect the bacteria, rather than the dye itself or its photoproducts. However, populations in contact with the dye and products of photocatalysis showed no significant difference from control. Some anthraquinone compounds, for example pigment red 177, are not acutely toxic by the oral route ($LD_{50} > 5000\,mg\,kg^{-1}$) [44]. In contrast, the anthraquinone dye Disperse Blue 3 has been determined to be toxic in bacterial, algal, and protozoan tests [48].

The results of this study indicate that the reaction intermediates are not toxic, which motivates the investigation of other degradation methods for comparison. However, it is also important to note that further investigations are necessary to obtain information on the synergistic effect of the relevant degradation products.

4. Conclusions

In the field of photocatalytic materials, ease of handling and efficiency in applications are the principal goals. For composites, synergistic effects between the constituent materials are additionally expected. TiO_2 possesses the ability to photodegrade organic compounds; however, it is such a fine powder that is difficult to handle. In this work, a composite material with the degradation ability of anatase and ease of handling was obtained using a carbon matrix that acts as an adsorbent. Glycerol was used as a binder for carbon and TiO_2 and was observed to improve the degree of crystallization of the anatase-phase TiO_2 at relatively low temperatures. Significant changes in the textural properties between the carbon and the composites were observed, such as increased density and a dramatic decrease in specific surface area. However, SEM revealed that in the composites, the carbon surface is not completely covered by TiO_2, leading to adsorption, which is even higher on the composite than on carbon per unit area. The most efficient composites were obtained from carbons with the largest specific surface areas and a suitable micropore–mesopore ratio, favoring the immobilization of a larger amount of TiO_2 particles, regardless the pH_{pzc} of the carbon. A perspective of this work is the preparation of a composite using carbon with acidic groups to favor the interaction with TiO_2. It is also foreseen to reduce the number of steps in the preparation of the TiO_2/C materials. The composites were able to degrade the dye AG25 under sunlight to the same extent as that under UV irradiation, removing nearly 100% of the dye in each case. A significant number of photodegradation products of the breaking of AG25 consisting of 3-methylbenzenesulfonic acid with different degrees of hydroxylation and other products absorbing in the visible-light range could be identified. The photodegradation product mixture and the dye were not toxic to an important plant-growth-promoting bacterium (*A. brasilense*) and even favored its growth due to the fact that several compounds can be used as alternative electron acceptors by numerous free-living bacteria, although many of these compounds are chemicals of environmental concern. Thus, the photodegradation process explored in this study presents an advantage over processes in which highly toxic byproducts are generated. We are also interested in optimizing the photocatalysis conditions under solar irradiation, in order to apply the composites in complex textile wastewater.

Acknowledgments

This work was supported by the following research projects: VIEP (ELGM-NAT09-G), CONACyT CB-2008-01-100439, and INFR-123779-2009. We thank the financial funding of the university (UAP) within the last project. Ricardo Agustín, Uriel Arroyo, Omar Ornelas, Patricia Ruíz, and Efraín Rubio are acknowledged for their assistance in different measurements. J.Z.P. is grateful for the grant received from VIEP and SNI (3501)–CONACyT.

References

[1] R. Leary, A. Westwood, Carbon 49 (2011) 741–772.
[2] G.L. Puma, A. Bono, D. Krishnaiah, J.G. Collin, J. Hazard. Mater. 157 (2008) 209–219.
[3] T.T. Lim, P.S. Yap, M. Srinivasan, A.G. Fane, Crit. Rev. Environ. Sci. Technol. 41 (2011) 1173–1230.
[4] K.Y. Foo, B.H. Hameed, Adv. Colloid Interface Sci. 159 (2010) 130–143.
[5] J. Matos, J.M. Chovelon, T. Cordero, C. Ferronato, Open Environ. Eng. J. 2 (2009) 21–29.
[6] M. Haro, L.F. Velasco, C.O. Ania, Catal. Sci. Technol. 2 (2012) 2264–2272.
[7] M.A. Rauf, S.S. Ashraf, Chem. Eng. J. 151 (2009) 10–18.
[8] J. Zhang, Z.H. Huang, Y. Xu, F.Y. Kang, Carbon-coated TiO_2 composites for the photocatalytic degradation of low concentration benzene, New Carbon Mater. 26 (2011) 63–70.
[9] A.R. Khataee, M. Zarei, M. Fathinia, M.K. Jafari, Desalination 268 (2011) 126–133.
[10] D. Huang, Y. Miyamoto, T. Matsumoto, T. Tojo, T. Fan, J. Ding, Q. Guo, D. Zhang, Sep. Purif. Technol. 78 (2011) 9–15.
[11] M. Asiltürk, Ş. Şener, Chem. Eng. J. 180 (2012) 354–363.
[12] S.A. Sabinas-Hernández, M.Sc. Thesis, Universidad Autónoma de Puebla, México, 2011.
[13] N.M. Mahmoodi, M. Arami, J. Zhang, J. Alloys Compd. 509 (2011) 4754–4764.
[14] Y.X. Chen, B.H. Luo, B.Y. Zhao, Y.J. Lai, H.Zh. Wang, M.Y. Gao, W.X. Zhang, K.B. Chen, J. Inorg. Organomet. Polym. 22 (2012) 90–96.
[15] O.J. Hao, H. Kim, P.-C. Chiang, Crit. Rev. Environ. Sci. Technol. 30 (2000) 449–505.
[16] A. Güngördü, A. Birhanli, M. Ozmen, Environ. Sci. Pollut. Res. Int. 20 (2013) 452–460.
[17] Opinion on Acid Green 25, Scientific Committee on Consumer Safety SCCS/1498/12, 2013, ISBN 978-92-79-31189-5, doi: 10.2772/58467 ND-AQ-13-024-EN-N.
[18] S. Figueroa, L. Vázquez, A. Alvarez-Gallegos, Water Res. 43 (2009) 283–294.
[19] M.B. Kasiri, A.R. Khataee, Desalination 270 (2011) 151–159.
[20] M. Saquib, M. Muneer, Color Technol. 118 (2002) 307–315.
[21] M.R. Ghezzar, F. Abdelmalek, M. Belhadj, N. Benderdouche, A. Addou, Appl. Catal. B: Environ. 72 (2007) 304–313.
[22] F. Bellanti, M. Castrucci, D. Ruiu, G. Visco, L. Campanella, Curr. Anal. Chem. 6 (2010) 100–110.
[23] D. Fabbri, P. Calza, A. Bianco Prevot, J. Photochem. Photobiol. A: Chem. 213 (2010) 14–22.
[24] H. Aydin, G. Baysal, Y. Bulut, Desalin. Water Treatment 2 (2009) 141–150.

[25] M.M. Dávila-Jiménez, M.P. Elizalde-González, V. Hernández-Montoya, Bioresor. Technol. 100 (2009) 6199–6206.
[26] N.M. Mahmoodi, B. Hayati, M. Arami, J. Chem. Eng. Data 55 (2010) 4638–4649.
[27] N.M. Mahmoodi, B. Hayati, M. Arami, C. Lan, Desalination 268 (2011) 117–125.
[28] W. Zhang, H. Li, X. Kan, L. Dong, H. Yan, Z. Jiang, H. Yang, Bioresour. Technol. 117 (2012) 40–47.
[29] B.H. Hameed, A.A. Ahmad, N. Aziz, Chem. Eng. J. 133 (2007) 195–203.
[30] Z. Wang, B. Xiang, R. Cheng, Y. Li, J. Hazard. Mater. 183 (2010) 224–232.
[31] R. Parimalam, V. Raj, P. Sivakumar, E.-J. Chem. 9 (2012) 1683–1698.
[32] O.S. Bello, Phys. Chem. 6 (2011) 141–145.
[33] N.M. Mahmoodi, B. Hayati, M. Arami, H. Bahrami, Desalination 275 (2011) 93–101.
[34] M.P. Elizalde-González, J. Mattusch, A.A. Peláez-Cid, R. Wennrich, J. Anal. Appl. Pyr. 78 (2007) 185–193.
[35] M.P. Elizalde-González, M.M. Dávila-Jiménez, O. Ornelas-Dávila, Patent ES2356765 (2011).
[36] S. Hara, Y. Hashidoko, R.V. Desyatkin, R. Hatano, S. Tahara, Appl. Environ. Microbiol. 75 (2009) 2811–2819.
[37] T. Sreethawong, S. Ngamsinlapasathian, S. Yoshikawa, Mater. Res. Bull. 47 (2012) 199–205.
[38] M.P. Elizalde-González, E. García-Díaz, S.A. Sabinas-Hernández, J. Hazard. Mater. 263 (2013) 73–83.
[39] L.F. Velasco, J.B. Parra, C.O. Ania, Adsorpt. Sci. Technol. 28 (2010) 727–738.
[40] S. Hisaindee, M.A. Meetani, M.A. Rauf, Trends Anal. Chem. 49 (2013) 31–44.
[41] U.G. Akpan, B.H. Hameed, J. Hazard. Mater. 170 (2009) 520–529.
[42] J. Xu, Y. Ao, D. Fu, Ch. Yuan, J Hazard. Mater. 164 (2009) 762–768.
[43] M. Constapel, M. Schellenträger, J.M. Marzinkowski, S. Gäb, Water Res. 43 (2009) 733–743.
[44] Eurocolour, Ecological and Toxicological Association of Dyes and Organic Pigments Manufacturers (ETAD). Colourants for Food Contact Plastics: Aspects of Product Safety, 4.21 Anthraquinone pigments, 2002, p. 49, Available from: www.cefic.be/files/Publications/FDL_en.pdf
[45] R.K. Suraj Singh, P.B. Mazumder, M.K. Bhatacharjee, G.D. Sharma, IOSR J. Pharm. Biol. Sci. 8 (2013) 20–24.
[46] M.A. Mascarúa-Esparza, R. Villa-González, J. Caballero-Mellado, Plant Soil 106 (1988) 91–95.
[47] G. Alexandre, Microbiology 156 (2010) 2283–2293.
[48] Č. Novotný, N. Dias, A. Kapanen, K. Malachová, M. Vándrovcová, M. Itävaara, N. Lima, Chemosphere 63 (2006) 1436–1442.